Applied Catalysis B: Environmental 224 (2018) 146–158

Contents lists available at ScienceDirect

Applied Catalysis B: Environmental

journal homepage: www.elsevier.com/locate/apcatb

Research Paper

Active and durable alkaline earth metal substituted perovskite catalysts for dry reforming of methane

Srikanth Dama, Seema R. Ghodke, Richa Bobade, Hanmant R. Gurav, Satyanarayana Chilukuri*

Catalysis Division, CSIR- National Chemical Laboratory, Dr. Homi Bhabha Road, Pune, 411008, India

ARTICLE INFO

Keywords:
Perovskites
Dry reforming
Citrate gel method
Nickel
Carbon deposition

ABSTRACT

Dry reforming of methane is an important process for the utilization of CO_2 and to get valuable synthesis gas. Alkaline earth metal substituted $MZr_{1-x}Ni_xO_{3-\delta}$ perovskites were synthesized by citrate gel method, characterized and evaluated for dry reforming methane. Characterization results show that the type of alkaline earth substituted at the A site of the perovskite oxide plays an important role in terms of structure, basicity, oxygen deficiency and Ni dispersion. Calcium substituted $CaZr_{0.8}Ni_{0.2}O_{3-\delta}$ catalyst shows superior activity in terms of high CH_4 and CO_2 conversion, while maintaining the activity even after 500 h of reaction. Mechanistic investigations were carried out using transient pulse experiments and insitu FTIR-diffuse reflectance spectroscopy. These experiments reveal that redox property and basicity play important role in activation and sustaining the reforming reaction. Insitu FTIR measurements show that surface hydroxyl groups of the support are vital for high activity and durability of $CaZr_{0.8}Ni_{0.2}O_{3-\delta}$ catalyst. XRD and TGA analysis of catalysts after reaction show the structures are retained, but peaks pertaining to coke were observed on $SrZr_{0.8}Ni_{0.2}O_{3-\delta}$ and $BaZr_{0.8}Ni_{0.2}O_{3-\delta}$ catalysts. On the otherhand, $CaZr_{0.8}Ni_{0.2}O_{3-\delta}$ catalyst had only amorphous carbon even after 500 h of reaction. HRTEM studies revealed that $SrZr_{0.8}Ni_{0.2}O_{3-\delta}$ and $BaZr_{0.8}Ni_{0.2}O_{3-\delta}$ catalysts deactivated mostly due to the formation of carbon nanotubes with Ni embedded in them. Raman and XPS analysis helped in identifying types of coke precursors present on the catalysts. The investigation also illustrate that type of carbon formed depends on the basicity of perovskite oxide, metal to support interaction, Ni crystallite size, surface hydroxyl groups and oxygen defects. This study clearly demonstrated that $CaZr_{0.8}Ni_{0.2}O_{3-\delta}$ is an excellent catalyst for dry reforming reaction with long life.

1. Introduction

The world is preparing to overcome the possible effects of global warming attributed to green house gas (GHG) emissions, particularly carbon dioxide emissions, as its level has crossed the 400 ppm level [1]. Hence, numerous initiatives are being taken for the development of CO_2 capture and utilization technologies that can help either to cap or reduce its level in the atmosphere. Similarly, CH_4 being another GHG; its release to the atmosphere is also a cause of concern. In recent times, various research programmes are proposed or initiated to utilize both these green house gases to obtain fuels and chemicals. Dry reforming of methane is one such programme that utilizes both CO_2 and CH_4 to give synthesis gas (syngas). Syngas is an important input for many chemicals and fuels. In dry reforming reaction, H_2/CO ratio of product syngas is low (≈ 1) and hence suitable for production of long chain hydrocarbons through Fischer-Tropsch (FT) synthesis [2,3].

$$CH_4 + CO_2 \leftrightarrow 2CO + 2H_2 \ (\Delta H^{\circ}_{298K} = +247 \text{ kJ/mol}) \quad (1)$$

In addition to main dry reforming reaction, reverse water gas shift reaction is also dominant under these conditions;

$$CO_2 + H_2 \leftrightarrow CO + H_2O \ (\Delta H^{\circ}_{298K} = +40.6 \text{ kJ/mol}) \quad (2)$$

However, to practice dry reforming commercially, the process faces some major challenges. Being highly endothermic reaction, it has to be conducted at high temperatures. As a consequence, catalysts are deactivated due to active metal sintering and coke formation [4]. Numerous investigations attempted to address these twin problems, mostly by using supported precious metal catalysts [5,6]. However, use of supported precious metal catalysts commercially involves high costs. Hence, nickel based catalysts are the best alternative, due to their comparable activity in dry reforming, abundant availability and relatively lower price. But, Ni based catalysts are more prone to deactivation due to carbon deposition and metal sintering. There were many reports on understanding of coke formation on Ni catalysts and how to fortify them to resist coke formation, inorder to get durable catalysts for dry reforming reaction [7].

* Corresponding author. Present address: Catalysis Division, CSIR-National Chemical Laboratory, Dr. Homi Bhabha Road, Pune, 411008, Maharashtra, India.
E-mail addresses: sv.chilukuri@ncl.res.in, satya.cvv@gmail.com (S. Chilukuri).

http://dx.doi.org/10.1016/j.apcatb.2017.10.048
Received 3 August 2017; Received in revised form 6 October 2017; Accepted 19 October 2017
Available online 19 October 2017
0926-3373/

The dry reforming reaction proceeds through CH_4 decomposition followed by oxidation of the carbon species. This mechanism requires bi-functional metal supported catalysts that can effectively catalyze CH_4 cracking and simultaneous removal of carbon species. In order to meet these requirements, high metal dispersion and resistance to metal sintering are essential, while redox property of the support helps to oxidize the carbon formed during the reforming process. Structured oxides like perovskites and hydrotalcites have been investigated for this reaction [8]. It is also reported that the metal catalysts can be promoted by using supports that consist of basic oxides/redox oxides [9,10]. Bi-metallic systems were also explored for improved activity and long term durability [11]. Addition of basic oxides to the support is expected to enhance the CO_2 activation and also helps in gasification of deposited carbon on the active sites [12]. In general, ZrO_2 is considered as a good support, because of its higher thermal stability and unique chemical properties like redox and acid-base functionality [13]. There were several reports dealing with Ni supported on ZrO_2, but most of them deactivated due to coke formation and sintering. Addition of promoters like CaO, MgO and CeO_2 is reported to help improve the catalyst stability [14].

Perovskite type oxides have a well defined structure and they can facilitate high metal dispersion, even on subjecting to severe oxidation-reduction processes at high temperatures [15]. Hence, efforts were made to synthesize catalysts that have active metals (transition metals like Ni or precious metals) incorporated in to the perovskite lattice and use them for DRM. In addition, substitution of Ca, Sr and Ba in the A site of perovskite lattice is expected to improve and help stabilize dry reforming activity of the catalyst. In this report, Ni is substituted in $MZrO_3$ (M = Ca, Sr and Ba) family of perovskite type oxides and their activity and durability was investigated for dry reforming (CH_4 + CO_2) reaction to obtain syngas. The perovskite oxides were synthesized using citrate gel method and characterized using XRD, Raman spectroscopy, BET surface area, CO chemisorption, CO_2-temperature programmed desorption (CO_2-TPD), O_2 −temperature programmed desorption (O_2-TPD), temperature programmed reduction (TPR), transient pulse technique and in-situ FTIR. Among the catalysts studied, Ca substituted perovskites were found to be more active in terms of CH_4 and CO_2 conversions and the activity was extraordinarily stable even after long hours (500 h) on stream. The carbon formed on these catalysts was investigated by XRD, TEM, TGA, XPS and Raman spectroscopy.

2. Experimental techniques

2.1. Preparation of the catalysts

The $MZr_{1-x}Ni_xO_{3-\delta}$ (M = Ca, Sr and Ba; x = 0 and 0.2) perovskite type oxides were prepared by conventional citrate gel method. Stoichiometric quantities of the corresponding metal nitrates were dissolved in minimum required water and added drop wise to the citric acid solution under constant stirring at 353 K. Following complexation, the solution was evaporated and dried at 453 K for 12 h to obtain spongy amorphous citrate gel. This fluffy material was crushed and calcined at 1023 K for 6 h in air flow to get the corresponding $MZr_{1-x}Ni_xO_{3-\delta}$ (M = Ca, Sr and Ba; x = 0 and 0.2) perovskite type oxides.

2.2. Characterization techniques

Powder X-ray diffraction (XRD) pattern of the $MZrO_3$ and Ni substituted $MZr_{1-x}Ni_xO_{3-\delta}$ perovskites were collected using PANalytical X'pert Pro dual goniometer diffractometer equipped with an X'celerator solid-state detector. Nickel filtered Cu Kα (1.5418 Å) radiation was used for the data collection using a flat holder in Bragg-Brentano geometry with 1° slit at the source side. The data were recorded in 2θ range (10–90°) in step size of 0.008°. Rietveld refinements of powder XRD pattern were carried out with the GSAS EXPGUI programme. Profile refinements utilized the pseudo-Voigt function. Initially, background and scale factors were refined by cell parameters and positional parameters. The mean crystallite sizes of the oxides were calculated using Debye–Scherrer equation.

High resolution transmission electron microscopy (HRTEM) investigations were conducted using a FEI Technai TF-30 instrument operating at 300 keV. Samples were prepared by dispersing them in isopropyl alcohol; a portion of this suspension was transferred onto carbon coated copper grids and allowed for natural drying at room temperature.

The Brunauer-Emmett-Teller (BET) surface areas of the samples were measured by nitrogen sorption at liquid nitrogen temperature (77 K) using a Quantachrome Autosorb iQ equipment. Prior to N_2 adsorption, the samples were degassed at 573 K for 3 h to remove any residual moisture and other volatiles.

Nickel dispersion was determined through CO chemisorptions of H_2 using Quantachrome Autosorb-iQ instrument. Prior to sorption, samples were reduced in-situ in H_2 stream at 773 K for 2 h. Following this, the samples were evacuated for 2 h at the same temperature and subsequently cooled to 313 K under evacuation to record CO adsorption isotherm. The isotherms include both physisorption and chemisorption portions. Chemisorbed CO uptakes were determined by extrapolating the linear portion of the isotherm to zero pressure. The dispersion of nickel was calculated under the assumption that the stoichiometry of CO/Ni (surface) is equal to 2.

Temperature programmed reduction (TPR) profiles were obtained using a Micromeritics Autochem 2920 catalyst characterization system, equipped with TCD detector. Freshly calcined samples were treated in 5% O_2-He gas mixture (30 ml min^{-1}) by ramping the temperature to 673 K at a heating rate of 5 K min^{-1}. Following this heat treatment for 1 h, the sample was cooled to 323 K in argon (purity 99.995%) flow. Subsequently, the gas was changed to 30 ml/min of 5% H_2 in Ar flow and the catalyst was heated to 1273 K at a heating rate of 5 K min^{-1}. The change in H_2 concentration at the outlet was monitored by TCD and plotted against temperature to yield TPR profiles. Water produced during the reduction process was condensed and collected in a cold trap.

Temperature programmed desorption of CO_2 (TPD- CO_2) was carried out to study the nature of basicity of the support using a Micromeritics Autochem 2920 equipped with a TCD detector. The samples were first degassed at 573 K in 40 ml min^{-1} of He flow for 60 min. Then the sample was cooled to 323 K in He, and the gas was switched to 30 ml min^{-1} of 10%CO_2 in He for 30 min. Following this, the sample was purged with He for 30 min by ramping the temperature to 373 K at 5 K/min in order to remove the physisorbed CO_2. Subsequently, the sample was heated at 10 K/min to 1273 K under He flow (40 ml/min) while monitoring the TCD signal for desorbed CO_2.

Temperature programmed desorption of O_2 (TPD- O_2) was carried out to study the defective sites in substituted perovskites using a Micromeritics Autochem 2920. Approximately 50 mg of the sample was filled in a U shape quartz tube and calcined in 5% O_2/Ar (30/min) at 773 K for 30 min. Following this, the sample was cooled to 373 K and gas was switched to 10% H_2 and heated to 773K to carry out reduction. Later, the sample was cooled to 313 K under He (30 ml/min) flow and exposed to 5% O_2/Ar for 30 min. Afterwards, the sample was purged in He (40 ml/min) for the removal of weakly adsorbed oxygen and TPD of O_2 was carried out by heating up to 1273 K at a ramping rate of 10 K/min.

In situ FTIR of the perovskite samples was carried out using Bruker Tensor 27 spectrometer in diffuse reflectance mode (DRIFT) equipped with MCT detector. Before the analysis, the sample was heated inside the diffuse reflectance cell in N_2 at 673 K to clean the surface. Following this, the sample was reduced in H_2/N_2 (1/4) mixture for 2 h and later the cell chamber was purged with N_2 at 673 K for 20 min while cooling the sample to room temperature. The dry reforming reaction was carried out by passing CH_4 + CO_2 mixture (30 ml/min) in 1:1 ratio through the sample in a DRIFT cell. The spectra were recorded at

Table 1
Structural and textural properties of $MZr_{1-x}Ni_xO_{3-\delta}$ (M = Ca, Sr and Ba; x = 0 and 0.2) perovskites. .

Formulae Space group	$CaZrO_3$ Pcmn (62)	$CaZr_{0.8}Ni_{0.2}O_3$ Pcmn (62)	$SrZrO_3$ Pm-3m	$SrZr_{0.8}Ni_{0.2}O_3$ Pm-3m	$BaZrO_3$ Pm-3m	$BaZr_{0.8}Ni_{0.2}O_3$ Pm-3m
a/Å	5.5920(1)	5.5911(9)	4.1005(2)	4.0920(4)	4.1900(4)	4.1878(6)
b/Å	8.0114(6)	8.0106(1)	4.1005(2)	4.0920(4)	4.1900(4)	4.1878(6)
c/Å	5.7505(1)	5.7502(9)	4.1005(2)	4.0920(4)	4.1900(4)	4.1878(6)
Rp (%)	6.2	5.6	6.3	6.4	6.3	7.6
WRp (%)	8.3	6.4	8.4	8.1	8.4	9.3
Chi^2	2.3	1.6	2.7	2.6	1.6	2.3
Surface area (m^2/g)	9.2	13.2	12.1	14.1	13.4	14.6
Tolerance factor[a]	0.91	0.92	0.94	0.95	1.00	1.01
Crystallite size (nm)	42	38	40	36	35	34
Ni dispersion (%)	–	13.5	–	4.0	–	3.9
Surface Ni metal area (m^2/g)	–	6.2	–	1.5	–	1.4
Average Ni crystallite size (nm)	–	7.2	–	25.0	–	25.6

[a] calculated using formulae $\tau = (r_A + r_O)/(\sqrt{2}(r_B + r_O))$.

temperatures 523, 573, 623 and 673 K, while monitoring the products formed using an online gas chromatograph (Thermo Scientific Trace 1110) equipped with a Spherocarb packed column (1/8" OD and 8 feet length). The DRIFT spectra of the reaction intermediates were obtained by the substraction of the background, which is recorded under N_2 flow. All the spectra recorded in Kubelka-Munk mode [16].

X-ray photoelectron spectroscopy (XPS) was carried using VG Scienta R3000HP spectrometer, equipped with a concentric hemispherical analyzer. Aluminium Kα monochromator source was used for excitation. Samples were mounted on a sample holder and evacuated in a preparation chamber. Subsequently, the sample was transferred to the analysing chamber and spectra were collected at a base pressure of 3×10^{-8} mbar. The binding energy (BE) was calibrated with respect to the C 1s value (285.0 eV) of contaminated carbon on the surface of the samples.

Raman spectra were recorded using Horiba JY Lab RAM HR 800 Czerny-Turner type spectrograph equipped with 800 mm focal length achromatic flat field monochromator and charge-couple device (CCD) detector. The wavelength region (200–2000 cm^{-1}) was scanned using a He-Ne laser (632.8 nm, 20 mW). Thermogravimetric analysis of coke deposited (spent catalyst) samples was carried out by heating the sample to 1273 K in air flow at 10 K min^{-1}, using Mettler Toledo TGA/SDTA 851 model instrument. The weight loss in a defined region was used to estimate the coke content.

2.3. Transient pulse study of CH_4 and CO_2 reactions

Transient pulse experiments of methane followed by CO_2 reaction on different catalysts was conducted using a Micromeritics Autochem 2920 temperature programmed characterization system coupled to a mass probe (Pfeiffer QMS 200). Typically, fresh calcined sample (100 mg) was held between quartz wool plugs in a U shaped quartz tube and pre-reduced in 5% H_2/Ar flow (30 ml/min^{-1}) at 873 K for 2 h. Followed by this pre-treatment, the sample was purged in He flow for 1 h. Subsequently, 0.5 ml of CH_4 was pulsed into He flow which was followed by CO_2 pulse (0.5 ml) at an interval of 8 min. Each experiment was conducted with four consecutive pulses of each gas, at three temperatures, viz., 873, 973 and 1073 K. Signals of m/z = 2, 28, 15, 18 and 44 were monitored corresponding to H_2, CO, CH_4, H_2O and CO_2 respectively. The contribution of CO_2 to the signal at m/z = 28 was subtracted to eliminate the errors of CO signal.

2.4. Evaluation of catalysts

The dry reforming reactions were carried out in a packed-bed tubular down flow reactor made up of Incolloy HT, after placing it in a programmable tubular furnace. All the gases (CH_4, CO_2 and N_2) used for the reaction were regulated by mass flow controllers (Brooks Instruments). In a typical experiment, 0.5 cm^3 (0.6–0.7 g) of catalyst particles in 0.3–0.5 mm range were mixed with 0.5 cc of same size quartz pieces and loaded in the reactor supported by ceramic wool plugs. The catalyst bed temperature was measured by means of a chromel-alumel thermocouple centered in the catalyst bed. Prior to reaction, catalyst was calcined at 673 K for 3 h and reduced in situ at 873 K for 6 h using 20% H_2 in N_2 gas mixture. Subsequently, the DRM reaction was carried using a gas mixture consisting of CH_4, CO_2 and N_2 in the volume ratio of 1:1:1; i.e. each gas maintained at a flow rate of 80 ml/min with total gas hourly space velocity at 28,800 h^{-1}. The catalytic activity was evaluated at different temperatures (873, 923, 948, 998, 1023 and 1073 K). The product gas mixture was analysed using an online gas chromatograph (Chemito 1000) equipped with a spherocarb packed column (1/8" OD and 8 feet length).

Methane and CO_2 conversions and the H_2/CO ratio were calculated using the gas composition estimated by GC and by employing the following formulae given in supporting information.

3. Results and discussion

3.1. Textural and structural characterization of catalysts

The BET surface areas and active metal (Ni) dispersions obtained through CO chemisorption of $MZr_{1-x}Ni_xO_{3-\delta}$ (M = Ca, Sr and Ba; x = 0 and 0.2) perovskite type catalysts has been listed in Table 1. Specific surface area of the $MZrO_3$ perovskite type oxides has increased with variation in alkaline earth cation down the group from Ca to Ba substituted oxides, with similar trend being observed even in case of Ni substituted samples. As a result, BET surface areas followed the order $CaZr_{0.8}Ni_{0.2}O_{3-\delta}$ < $SrZr_{0.8}Ni_{0.2}O_{3-\delta}$ < $BaZr_{0.8}Ni_{0.2}O_{3-\delta}$; for x = 0 and 0.2. Surface areas of the samples increased to a little extent on Ni substitution, which is attributed to a small reduction in crystallite size. This was clearly seen from crystallite sizes calculated with the help of Debye–Scherrer equation using XRD line widths. The Ni metal dispersion on $CaZr_{0.8}Ni_{0.2}O_{3-\delta}$ perovskite type catalyst was higher compared to Sr and Ba perovskite catalysts, i.e. more active metal (Ni) is present on the surface of $CaZr_{0.8}Ni_{0.2}O_{3-\delta}$ perovskite. However, Ni impregnated on $CaZrO_3$ catalyst shows lower metal dispersion (5.1%) as compared to Ni substituted $CaZrO_3$ perovskite catalysts ($CaZr_{0.8}Ni_{0.2}O_{3-\delta}$).

3.2. X-ray diffraction

Fig. 1A shows X-ray diffraction pattern of freshly calcined $MZr_{1-x}Ni_xO_{3-\delta}$ (M = Ca, Sr and Ba; x = 0 and 0.2) perovskite oxide samples obtained by citrate gel method. The spectra reveal that on changing substitution from Ca to Ba, the number of diffraction lines decreased

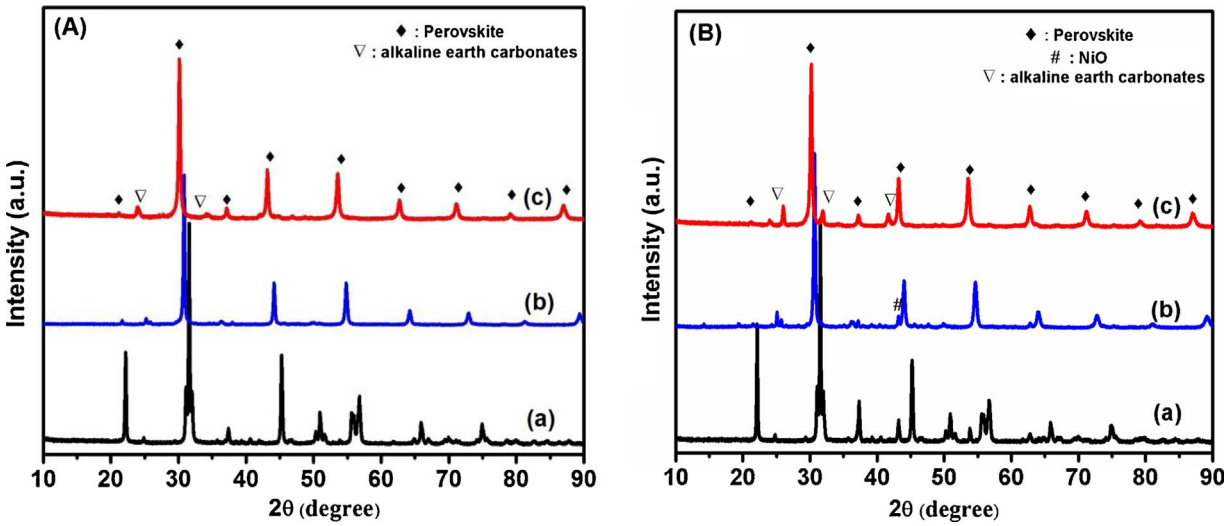

Fig. 1. XRD pattern of $MZr_{1-x}Ni_xO_{3-\delta}$ perovskites; (A) x = 0 and (B) x = 0.2; where M = (a) Ca, (b) Sr and (c) Ba.

indicating phase transition from orthorhombic to cubic. Additionally, respective alkaline earth carbonate impurities, which were not decomposed during the calcination, were observed in the spectra.

The cell parameters calculated from the XRD refinement are in good agreement with literature data (JCPDS −PDF No. 76-2401, 75-0467and 74-1299). Both Sr and Ba substituted perovskites crystallized in cubic phase, while cell parameter of Ba substituted sample increased compared to Sr substituted sample.

In the case of Ni substituted perovskites ($MZr_{0.8}Ni_{0.2}O_{3-\delta}$), the diffraction pattern clearly shows that the parent perovskite structural phase is retained on Ni substitution as shown in Fig. 1B. Some minor peaks observed in the 2θ range of 25–30° are assigned to the respective alkaline earth carbonate impurities and small amount of NiO (θ = 43.2°) on the surface. The intensity of impurity peaks increased on substitution of Ni. Moreover, the Rietveld refinement results reveal that after Ni substitution into Zr site, the lattice parameter decreased, indicating the incorporation of Ni into the perovskite lattice. A fraction of NiO also appears to be well dispersed on the surface. The decrease in lattice parameter is explained on the basis of smaller Ni^{+2} (69 pm) replacing the larger Zr^{+4} (72 pm), with the same coordination number (VI). Thus, it appears that the Ni in these samples is present in two forms; i.e (i) Ni substituted in the bulk of perovskite lattice and (ii) a small fraction of Ni is highly dispersed on the surface. The stability and distortion in ideal ABO_3 cubic perovskite structure is determined by tolerance factor (τ). The tolerance factor for Ca substituted sample is somewhat deviated from ideal value (~1). Hence, this perovskite is crystallized in orthorhombic phase (space group: Pcmn (62)).

$$\tau = (r_A + r_O)/(\sqrt{2}(r_B + r_O))$$

where r_A, r_B and r_O are the ionic radii of A, B and O ions. The cell parameters, surface areas and tolerance factors are given in Table 1.

3.3. Raman spectroscopy

The Raman spectra of calcined $MZrO_3$ (M = Ca, Sr and Ba) samples are given in Fig. 2. They show that the number of vibration modes decreased during the orthorhombic to cubic phase transition from Ca to Ba substituted perovskites. In case of $CaZrO_3$, which has orthorhombic Pcmn (62) phase, it is theoretically expected to have 24 Raman active modes. But, some modes may not be detectable due to their low polarizability or some modes could be hidden in highly intense bands [17]. Hence, we observe only 10 modes of vibrations in the 80–600 cm^{-1} region (Fig. 2). Also, at higher frequencies, the Raman peaks are broad due to second order scattering, resulting in the

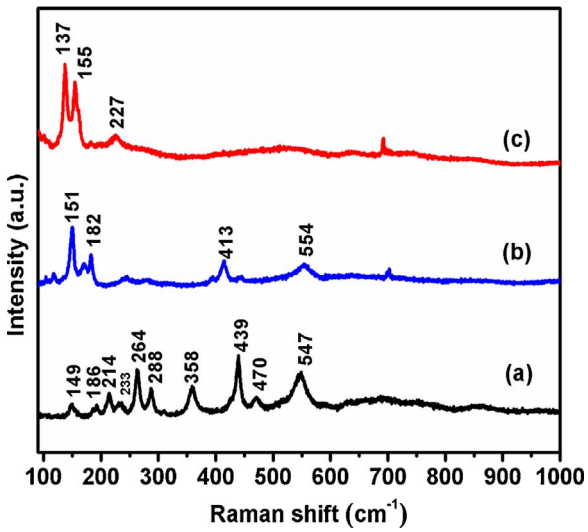

Fig. 2. Raman spectra of $MZrO_3$ perovskites; where M = (a) Ca, (b) Sr and (c) Ba.

Table 2
Raman vibration modes of $CaZrO_3$ type perovskite oxides. .

Our work (Γ cm^{-1}) Mode	K. Boobalan et al. [18] (Γ cm^{-1})	Martine Tarrida et al. [19] (Γ cm^{-1})	Orera et al. [20] (Γ cm^{-1})	Perry et al. [21] (Γ cm^{-1})
149 A_g	121, 147	145, 151, 172	145	153
186 B_{2g}	183	185		186
214 B_{2g}	212	213, 229	212, 227	
233 B_{2g}		235	234	228
264 A_g	262	263	262	
288 A_g	283	287, 310	286, 305	
358 A_g	356	358, 423	358, 418	340
439 $A_g + B_{1g}$	437	439	439	377, 418
470 B_{2g}	469	470	469	515
547 B_{1g} or B_{3g}	546	548	543	551

superposition of different combination modes. The frequencies of the observed Raman bands and their modes are listed in Table 2 and all are in agreement with reported data [18–21]. The shapes of the Raman bands indicate that the $CaZrO_3$ particles exist in nano regime as confirmed by XRD. The grain size of the perovskite is inversely proportional to the half width at half height of the Raman bands [18].

On the otherhand, Raman bands corresponding to carbonate

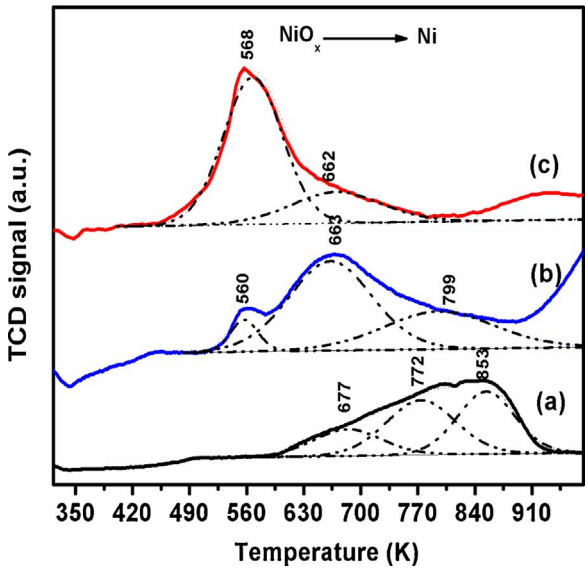

Fig. 3. Deconvoluted TPR profile of (a) $CaZr_{0.8}Ni_{0.2}O_{3-\delta}$ (b) $SrZr_{0.8}Ni_{0.2}O_{3-\delta}$ and (c) $BaZr_{0.8}Ni_{0.2}O_{3-\delta}$ perovskites.

impurities (151,182, 413,554 and 155,227) only were seen for $SrZrO_3$ and $BaZrO_3$ perovskites. Since, these samples crystallized in cubic phase (Pm3m), it is expected to have 12 vibrations, but all of them are forbidden Raman transitions [22]. The spectra of Ba and Sr based carbonates are similar, but considering the difference in their atomic mass (137.33 for Ba and 87.62 for Sr) bathochromic shift is expected in the case of Ba carbonate. The Raman bands of carbonates are very narrow; revealing covalent bonding of CO_3 vibrational units with no disorder [23]. These carbonates were earlier confirmed by XRD.

3.4. Temperature programmed reduction

The reduction properties of Ni substituted perovskites were investigated by H_2-TPR. Fig. 3 shows deconvoluted TPR profiles of three regions of hydrogen consumption observed for $CaZr_{0.8}Ni_{0.2}O_{3-\delta}$ and $SrZr_{0.8}Ni_{0.2}O_{3-\delta}$ zirconium perovskite oxides. In case of $BaZr_{0.8}Ni_{0.2}O_{3-\delta}$, only two peaks were seen. Bai et al. also observed similar TPR peaks in the 503–603K temperature range, which were attributed to the reduction of NiO [24]. Rudolfo et al. also reported a 573 K reduction peak belonging to the amorphous NiO on surface [25]. The low temperature peak corresponds to the reduction of weakly interacting NiO species, which are present on the perovskite surface.

In the case of $CaZr_{0.8}Ni_{0.2}O_{3-\delta}$ and $SrZr_{0.8}Ni_{0.2}O_{3-\delta}$ samples, peaks at 772K and 683K may be assigned to the reduction of NiO_x species, which are present on surface and sub surface region of the perovskite. The high temperature peaks above 783K are assigned to the NiO_x species, which are part of bulk perovskite lattice (Zr^{+4}-O-Ni^{+2}). Above 823K, reduction of carbonate impurities of Sr and Ba samples has been observed, whose presence was confirmed by Raman and XRD spectra. On close observation of TPR profiles of $CaZr_{0.8}Ni_{0.2}O_{3-\delta}$, it is clear that the peaks appear at higher temperatures compared to other two catalysts. The evolution of reduction peak at high temperature indicates rather a strong interaction of Ni with the perovskite structure; this can reduce the sintering during the reaction.

3.5. Temperature programmed desorption of CO_2 and O_2

The nature of surface basicity and strength were determined using CO_2-TPD, these results are illustrated in Fig. 4A. Since CO_2 is an acidic gas, basic support is expected to adsorb and promote its activation. It can be seen that all the samples show CO_2 desorption at high temperatures; therefore carbonate species must have formed on exposing the sample to CO_2. The CO_2-TPD profiles indicate that strength of basicity increased from Ca to Ba substituted perovskite samples. The $CaZr_{0.8}Ni_{0.2}O_{3-\delta}$ sample has shown sharp desorption peak in the 773-1023K temperature region. In case of $SrZr_{0.8}Ni_{0.2}O_{3-\delta}$ and $BaZr_{0.8}Ni_{0.2}O_{3-\delta}$ perovskites, the peaks were at higher temperatures (around 1073 K), as the corresponding $SrCO_3$ and $BaCO_3$ are decomposed only at higher temperatures [26,27].

Since the gas-solid reaction occurs over the perovskite surface, the amount of carbonate formation is expected to be related to surface area of the perovskite. The CO_2-TPD spectra of $CaZr_{0.8}Ni_{0.2}O_{3-\delta}$ indicate that CO_2 is adsorbed on the surface at lower temperature and is subsequently activated with ease. This activation is expected to play a key role in the elimination of carbon during dry reforming of methane. Further, on Sr and Ba substituted perovskites, the carbonate desorption peaks are broader and shifted to very high temperatures. Yan et al. [28] also observed similar results in case of $Ba_xSr_{1-x}Co_{0.8}Fe_{0.2}O_3$ and have observed higher CO_2 adsorption with increased Ba doping. Finally, CO_2-TPD results confirm that CO_2 is adsorbed on the perovskite surface and react with perovskite material forming carbonate species which decompose at high temperatures (> 923K). The shape of the TPD peak is asymmetric, indicating that desorption rate follows first order kinetics. The CO_2 desorption activation energy can be calculated following the Chan-Aris-Weinberg method [29].

$$E_d = RT_m\left[-1 + \sqrt{1 + 5.832\left(\frac{T_m}{W_{1/2}}\right)^2}\right]$$

where R is the gas constant, T_m is the maximum temperature of TPD peak and $W_{1/2}$ is the peak width at half maximum and E_d is the activation energy of the desorption (directly proportional to T_m). The calculated activation energy values of CO_2 desorption from different alkaline earth substituted perovskites are in the order:

Ca (55.9 kcal mol^{-1}) < Sr (84.2 kcal mol^{-1}) < < Ba (more than 84.2 kcal mol^{-1})

The O_2–TPD MS experiments help to identify oxygen defect sites in the perovskite lattice unambiguously. In this experiment the temperature is raised in programmed way which will lead to the release of the oxygen from the lattice associated with lower valence cations (Ni^{+2}/Ni^{+3}) that were substituted in place of high valence (Zr^{+4}) cations, as the perovskite lattice must compensate for the charge imbalance [30]. This charge imbalance creates oxygen defects/vacancies. This charge compensation phenomenon is more important under reducing atmosphere. The O_2-TPD experiments were carried out for all the Ni substituted catalysts and is shown in Fig. 4B. For $CaZr_{0.8}Ni_{0.2}O_{3-\delta}$ sample, the oxygen desorption peak has been observed in temperature range of 873–1073 K. But in case of $SrZr_{0.8}Ni_{0.2}O_{3-\delta}$ and $BaZr_{0.8}Ni_{0.2}O_{3-\delta}$ perovskites, O_2 desorption peak shifted to > 1073 K, while their intensity's were lower compared to Ca substituted perovskite (see Fig. S1A). The loss of lattice oxygen at elevated temperature leads to increase in the volume of the unit cell or decrease in the density of unit cell [31]. Moreover, passing over from Ca to Ba substituted samples, the amount of O_2 adsorption decreases drastically, with the peak areas following the order $CaZr_{0.8}Ni_{0.2}O_{3-\delta}$ > $SrZr_{0.8}Ni_{0.2}O_{3-\delta}$ > $BaZr_{0.8}Ni_{0.2}O_{3-\delta}$. Higher concentration of defective sites in terms of adsorbed O_2 is favourable in terms of resistance to carbon formation during dry reforming reaction. Consequently $CaZr_{0.8}Ni_{0.2}O_{3-\delta}$ perovskite catalyst should have more ability to provide oxygen vacancies and improved donation of lattice oxygen from bulk to surface, which is useful for removal of carbon. On the otherhand, Ni impregnated catalysts (Ni/$CaZrO_3$) show less oxygen vacancies as compared to $CaZr_{0.8}Ni_{0.2}O_{3-\delta}$ perovskite catalysts (see Fig. S1B).

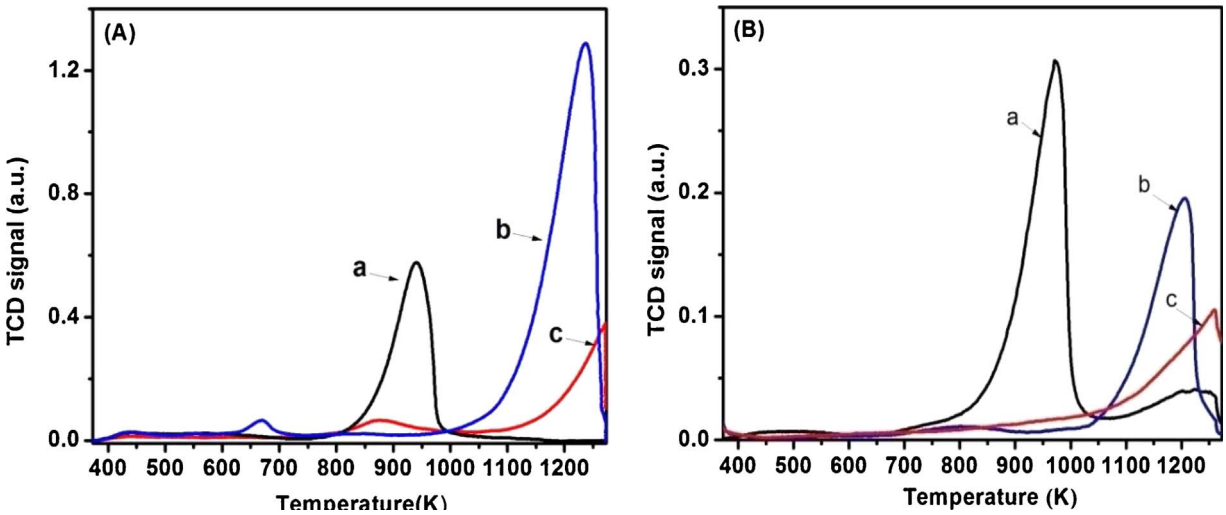

Fig. 4. TPD of (A) CO_2 and (B) O_2 profile of $MZr_{0.8}Ni_{0.2}O_{3-\delta}$ perovskites, where M = (a) Ca, (b) Sr and (c) Ba.

3.6. Catalytic performance of alkaline earth substituted $MZr_{0.8}Ni_{0.2}O_{3-\delta}$ catalysts

The perovskite type oxides containing Ni and different A site cations (Ca, Sr and Ba) were evaluated as catalysts for their performance in dry reforming of methane.

3.6.1. Effect of temperature over $MZr_{0.8}Ni_{0.2}O_{3-\delta}$ (M = Ca, Sr and Ba) catalysts

The reaction temperature plays a vital role in influencing the catalytic activity. Moreover, the basicity, active metal dispersion and presence of oxygen defects are also expected play important role in changing the activity. The CO_2 reforming of methane was studied over the three $MZr_{0.8}Ni_{0.2}O_{3-\delta}$ (M = Ca, Sr and Ba) perovskite type oxide catalysts followed by in-situ reduction under H_2 at 873K. Conversion of CH_4 and CO_2 as a function of reaction temperature is given in Fig. 5A and B respectively.

Both CH_4 and CO_2 conversions increased with temperature, with a sharp rise in the 873–1073K temperature zone. At higher reaction temperatures, the CO_2 conversion was slightly higher than CH_4 conversion, leading to a lower H_2 to CO ratio (< 1) of the output syngas. If DRM reaction occurred stoichiometrically, the H_2/CO ratio would have been equal to unity. But, at higher temperatures, the side reactions like reverse water gas shift reaction (RWGS) and reverse Boudouard reaction must be prevalent resulting in H_2/CO ratio < 1. As a result of these side reactions, additional CO is produced, leading to lower H_2/CO ratio. There were several studies that reported such observations during dry reforming reaction [32].

$$CO_2 + H_2 \leftrightarrow CO + H_2O \ (\Delta H^{\circ}_{298K} = 40.6 \text{ kJ mol}^{-1}) \quad (2)$$

$$CO_2 + C(s) \leftrightarrow 2CO \ (\Delta H^{\circ}_{298K} = 171 \text{ kJ mol}^{-1}) \quad (3)$$

The $CaZr_{0.8}Ni_{0.2}O_{3-\delta}$ catalyst shows relatively higher CH_4 and CO_2 conversions compared to $SrZr_{0.8}Ni_{0.2}O_{3-\delta}$ and $BaZr_{0.8}Ni_{0.2}O_{3-\delta}$ substituted perovskite catalysts. As equilibrium conversion was achieved at 1073 K, this temperature was chosen for further studies.

3.6.2. Durability of $MZr_{0.8}Ni_{0.2}O_{3-\delta}$ (M = Ca, Sr and Ba) catalysts during DRM

It is generally reported that DRM catalysts deactivate rapidly due to the formation of coke that blocks the active metal sites. The coke formation occurs as a result of side reactions such as methane cracking and CO disproportionation (Boudouard) reactions. Hence, the durability of the above catalysts was investigated for 12 h on stream, under optimized dry reforming conditions: GHSV 28,800 h^{-1}; CH_4:CO_2:N_2 (1:1:1), temperature, 1073K; atmosphere pressure. The results of this

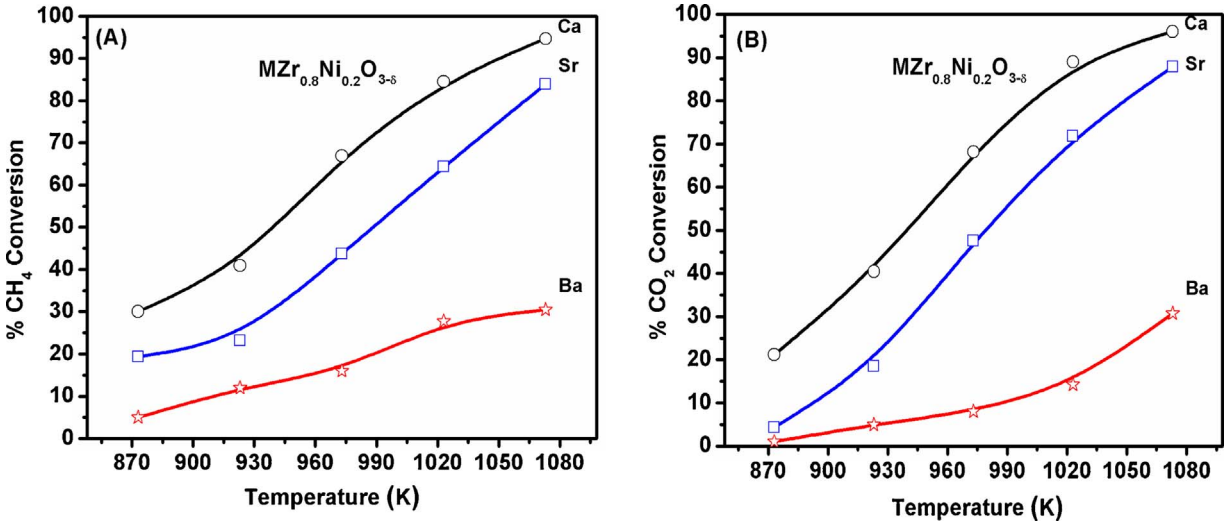

Fig. 5. Influence of temperature over $MZr_{0.8}Ni_{0.2}O_{3-\delta}$ catalysts in DRM of methane; (A) CH_4 conversion and (B) CO_2 conversion; M = Ca, Sr and Ba. Reaction conditions: $CH_4/CO_2/N_2$ = 80/80/80, GHSV = 28,800 h^{-1} at 1 atm.

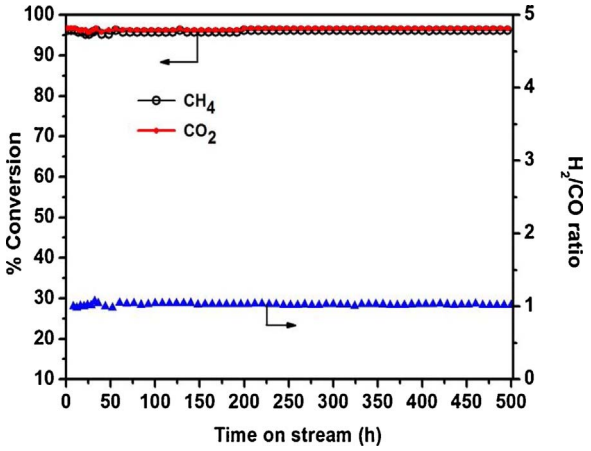

Fig. 6. Long term durability study of the $CaZr_{0.8}Ni_{0.2}O_{3-\delta}$ catalyst in DRM reaction. Reaction conditions: $CH_4/CO_2/N_2$ = 80/80/80, GHSV = 28,800 h^{-1}, Temp. 1073 K at 1 atm.

experiment are given in Fig. S2A and S2B . The $CaZr_{0.8}Ni_{0.2}O_{3-\delta}$ catalyst showed stable CH_4 and CO_2 conversions of 95 and 96% respectively without any noticeable drop in the activity. On the otherhand, both $SrZr_{0.8}Ni_{0.2}O_{3-\delta}$ and $BaZr_{0.8}Ni_{0.2}O_{3-\delta}$ perovskite catalysts deactivated with time. To understand this deactivation process, spent catalysts were characterized after 12 h of time on stream, using various techniques to analyse the quantity and nature of carbon deposited over them.

3.6.3. Comparison of catalytic activity over Ni substituted $CaZrO_{3-\delta}$ and Ni impregnated ($Ni/CaZrO_3$) catalysts

The above discussed results demonstrate that $CaZr_{0.8}Ni_{0.2}O_{3-\delta}$ perovskite derived oxide is a good catalyst for DRM reaction. Hence, it will be interesting to understand the role of substituted Ni in the reaction. Hence, a Ni impregnated (6 wt%) catalyst was prepared by using $CaZrO_3$ perovskite oxide as the support (details are given in supporting information S1) and compared its performance with Ni substituted perovskite oxide catalyst prepared through citrate gel method. Fig. S3 shows that the activity of Ni substituted perovskite oxide ($CaZr_{0.8}Ni_{0.2}O_{3-\delta}$) catalyst is much better compared to impregnated ($Ni/CaZrO_3$) catalyst. Moreover, the CO_2 conversion is relatively higher

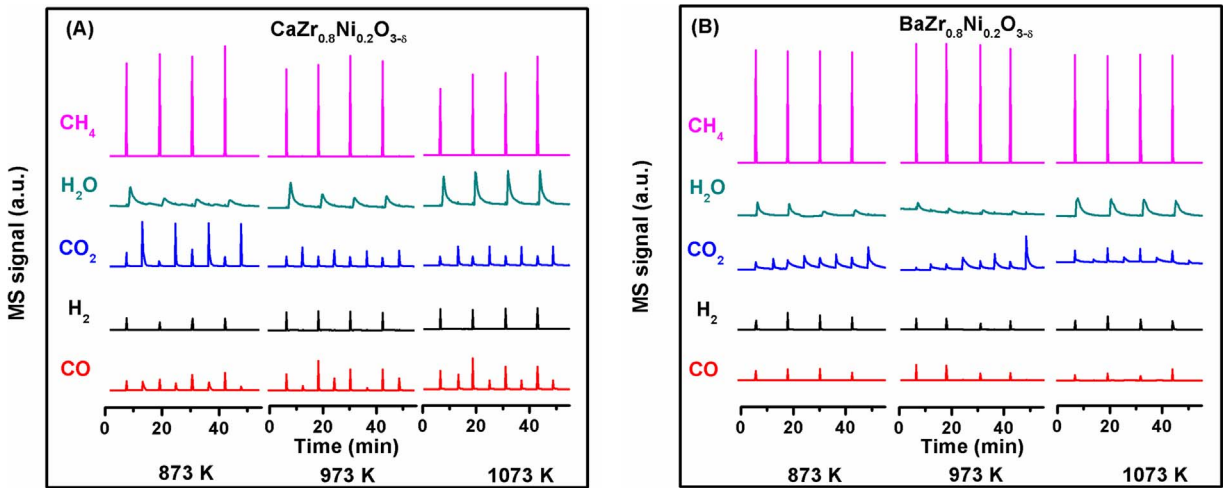

Fig. 7. MS signal during pulse experiment of (A) $CaZr_{0.8}Ni_{0.2}O_{3-\delta}$ and (B) $BaZr_{0.8}Ni_{0.2}O_{3-\delta}$ catalyst in DRM reaction.

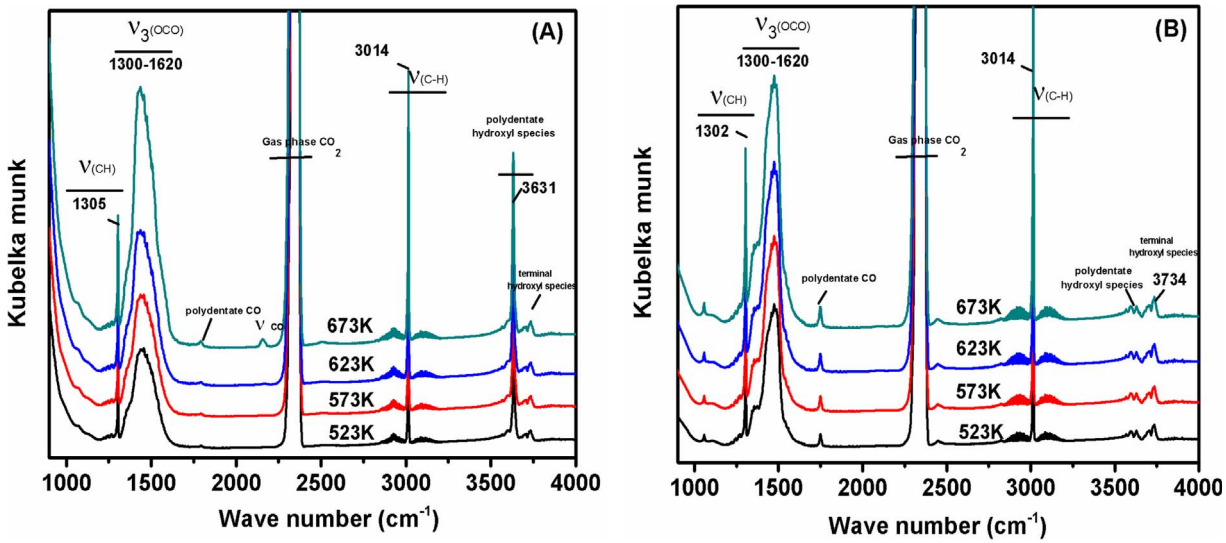

Fig. 8. Insitu FTIR spectra of various species present during the reaction between CH_4 and CO_2 over $MZr_{0.8}Ni_{0.2}O_{3-\delta}$ catalysts at different temperatures; (A) $CaZr_{0.8}Ni_{0.2}O_{3-\delta}$ and (B) $BaZr_{0.8}Ni_{0.2}O_{3-\delta}$.

compared to CH_4 conversion on impregnated catalyst. This in turn led to lower H_2/CO ratios (< 1). In terms of stable activity of catalysts in the form of CH_4 and CO_2 conversions, both catalysts appear to be similar. But, impregnated catalyst is expected to coke at a faster rate, if the reaction would have been continued for a longer duration, as a result of side reactions. High rate of coking on impregnated catalyst is expected due to lower Ni dispersion (Section 3.1) and less oxygen vacancies (Section 3.5) as compared to $CaZr_{0.8}Ni_{0.2}O_{3-\delta}$ catalyst.

3.6.4. Long term durability of $CaZr_{0.8}Ni_{0.2}O_{3-\delta}$ catalyst

Since, $CaZr_{0.8}Ni_{0.2}O_{3-\delta}$ catalyst showed excellent catalytic activity and attained equilibrium CH_4 and CO_2 conversions, its durability was checked for 500 h. Its performance depicted in Fig. 6, shows that both CH_4 and CO_2 conversions remained stable and almost constant at about 95 and 96%, respectively upto 500 h. The H_2/CO molar ratio was also close to unity. The stable activity of $CaZr_{0.8}Ni_{0.2}O_{3-\delta}$ could be attributed either to the low amount of carbon formed on the surface of the catalyst or the type of carbon formed does not block the active sites of the catalysts during the reaction. Moreover, the well dispersed active metal must not have sintered significantly. Probably, the oxygen defects created due to Ni substitution might have also been helpful for the removal of coke formed thus imparting durability to the catalyst.

3.6.5. Transient pulse experiments

Mass spectral signals of transient pulse experiments are shown in Fig. 7A and B. On $CaZr_{0.8}Ni_{0.2}O_{3-\delta}$ and $BaZr_{0.8}Ni_{0.2}O_{3-\delta}$ perovskite catalysts, H_2 species were detected as soon as CH_4 was pulsed into the reaction chamber, indicating that CH_4 decomposition takes place over active Ni sites. More importantly, H_2O signal was observed though with hysteresis as compared to H_2, CO, CO_2 and CH_4 signals. Moreover, the intensity of the H_2O signal increased at higher reaction temperatures (see Fig. S4). This clearly suggests that CH_4 decomposition increased with temperature and thus formed hydrogen reacts with surface oxygen species to generate hydroxyl species. These hydroxyl species on dehydration form water. The hysteresis could be due to the slower reaction rate of dehydration reaction compared to other reactions. Upon pulsing methane; CO and CO_2 species were detected, which might have been generated by the reaction between lattice oxygen of perovskite and the carbon species. The intensities of CO and CO_2 signals were much stronger in case of $CaZr_{0.8}Ni_{0.2}O_{3-\delta}$ perovskite catalyst compared to $BaZr_{0.8}Ni_{0.2}O_{3-\delta}$, which may be interpreted for its higher active metal dispersion (see Table 1). CH_4 decomposition over Ni^0 sites produces adsorbed CH_x and H species; the latter species combine with each other and leave the surface as H_2. Finally, after complete decomposition of CH_4, the resultant carbon species is oxidized to CO and CO_2 at the interface of Ni and support oxide [6,33], leading to the generation of surface oxygen vacancies. These vacant sites are positively charged and posses high affinity towards oxygen. When CO_2 interacts with the oxygen vacancies, it results in the breaking of C—O bond leading to the decomposition of CO_2 with simultaneous compensation of oxygen to vacant sites. These processes indicate that both metal and redox properties of $CaZr_{0.8}Ni_{0.2}O_{3-\delta}$ perovskite are important for achieving high activity of the catalyst and also to retain it for long hours. In case of $BaZr_{0.8}Ni_{0.2}O_{3-\delta}$ catalyst, CO formation was not observed on pulsing of CO_2 and the intensity of CO_2 signal at the outlet was less intense probably due to its stronger adsorption on the catalyst. The higher intensity of CO signals after the CO_2 pulsing over $CaZr_{0.8}Ni_{0.2}O_{3-\delta}$ perovskite indicates ease of dissociation of CO_2 at oxygen vacant sites and deposition of inactive carbon over the active metal that can be easily removed by CO_2 via reverse boudouard reaction. Absence of CO signals during pulsing of CO_2 on $BaZr_{0.8}Ni_{0.2}O_{3-\delta}$ catalyst might be related to the nature of carbon formed and this carbon may be encapsulating surface Ni leading to deactivation of catalyst.

3.6.6. Insitu FTIR studies

Insitu FTIR experiments were conducted initially in N_2 flow at 298 K to study various vibrations of the sample that were used as background spectra. Subsequently, the reaction mixture containing CH_4 and CO_2 in 1:1 ratio was sent through the sample and spectra were recorded in the temperature range of 523–673 K, at 50 K intervals. Fig. 8A and B shows different species present over the catalysts $CaZr_{0.8}Ni_{0.2}O_{3-\delta}$ and $BaZr_{0.8}Ni_{0.2}O_{3-\delta}$ at various temperatures.

There are significant differences in the type of species present over $CaZr_{0.8}Ni_{0.2}O_{3-\delta}$ and $BaZr_{0.8}Ni_{0.2}O_{3-\delta}$ catalysts, which were better evident with increasing temperature. A major difference was observed in the intensities of the hydroxyl species ($\sim 3630\ cm^{-1}$) and formate type intermediates (1590 and $1365\ cm^{-1}$), which were higher on $CaZr_{0.8}Ni_{0.2}O_{3-\delta}$ as compared to $BaZr_{0.8}Ni_{0.2}O_{3-\delta}$. These differences show that coke accumulation follows different mechanistic pathways on these catalysts during the DRM depending on the nature of substituted alkaline earth cation at A site. Aparicio et al. reported use of transient techniques employing isotopically labelled reactants over Ru supported on silica and alumina samples. According to them, the nature of the support influences the reactant residence time [34]. On catalysts that are supported on alumina, a complex reaction network is involved during DRM reaction, in which hydroxyl groups are continuously supplied by the support to the active Ru metal-Al_2O_3 interface, which effectively can remove the carbon species [16]. Similar features were observed in the present investigation over $CaZr_{0.8}Ni_{0.2}O_{3-\delta}$ catalyst. On CH_4 decomposition over Ni sites, hydrogen atoms are produced and also consumed by perovskite for the formation of hydroxyl species that are observed in the range of 3600–3650 cm^{-1}. Subsequently, reaction takes place between adsorbed H and OH species leading to the formation of H_2O and desorption of CO as illustrated below:

CH_4 activation on metal surface

$$CH_4 \longrightarrow CH_{3(metal)} - ads + H_{(metal)} - ads$$
$$2H_{(metal)} - ads \leftrightarrow H_2\,(g)$$
$$OH_{(support)} - ads \leftrightarrow OH_{(metal)} - ads$$
$$OH_{(metal)} - ads \leftrightarrow O_{(metal)} - ads + H_{(metal)} - ads$$
$$H_{(metal)} - ads + OH_{(metal)} - ads \leftrightarrow H_2O(g)$$
$$CHx_{(metal)} - ads + O_{(metal)} - ads \leftrightarrow CO_{(metal)} - ads + xH_{(metal)} - ads$$
$$CO_{(metal)} - ads \leftrightarrow CO(g)$$

The H atoms upon CH_4 decomposition over metal surface spill over on to the surface of support.

Surface diffusion of H_2 $2H_{(metal)} - ads \leftrightarrow 2H_{(support)} - ads$

After adsorption of CO_2 on the catalyst surface, CO_2 reacts with surface oxide/hydroxyl species to form carbonate/bicarbonate species.

Carbonate formation

$$CO_2\,(g) \leftrightarrow CO_{2(support)} - ads$$
$$CO_{2(support)} - ads + O^{-2}{}_{(support)} \leftrightarrow CO_3{}^{-2}{}_{(support)} - ads$$
$$CO_{2(support)} - ads + OH^{-}{}_{(support)} \leftrightarrow HCO_3{}^{-}{}_{(support)} - ads$$

Finally carbon monoxide is released into gas phase from adsorbed intermediate species (formates) which is formed by reaction between CO_2 and hydrogen/hydroxyl species on the perovskite surface. These formate species decompose to release CO.

Formation and decomposition of formate intermediates

$$CO_3{}^{-2}{}_{(support)} - ads + 2H_{(support)} - ads \leftrightarrow HCO_2{}^{-}{}_{(support)} - ads + OH^{-}{}_{(support)}$$
$$HCO_3{}^{-}{}_{(support)} - ads + 2H_{(support)} - ads \leftrightarrow HCO_2{}^{-}{}_{(support)} - ads + H_2O_{(support)} - ads$$
$$HCO_2{}^{-}{}_{(support)} - ads \leftrightarrow CO_{(support)} - ads + OH^{-}{}_{(support)}$$
$$CO_{(support)} - ads \leftrightarrow CO(g)$$

FTIR studies show that increase in the residence time of carbonaceous intermediates on the surface of active metal leads to its polymerisation and eventually graphitization of carbon takes place over the active Ni metal.

After collection of spectra using dry reforming reaction mixture, strong intense bands in the 1300–1620 cm^{-1} region were seen for both the Ca and Ba substituted catalysts, which are attributed to carbonate and bicarbonate species (Fig. 8). The main bands in the spectra with high intensities may be attributed to the gaseous adsorbed species of (i) C—H vibrations of CH_4 at 3014 $cm^{-1}$and 1305 cm^{-1}, (ii) CO_2 gaseous rotation-vibrations of P band at 2360 cm^{-1} and R band at 2340 cm^{-1}. On increasing the temperature, additional bands are generated at 1800 cm^{-1} and 1747 cm^{-1} which are assigned to the CO stretching vibrations of polydentate or bridged carbonate species present on the surface [35]. In case of $CaZr_{0.8}Ni_{0.2}O_{3-\delta}$ perovskite, a small peak was seen at 2000–2200 cm^{-1} assigned to the gaseous CO formation at 673 K which is also confirmed by online GC analysis. Fig. S5 illustrates the deconvolution of FTIR bands of Ca and Ba perovskite in the 1300–1620 cm^{-1} region obtained at 673 K. These deconvoluted bands of Ca perovskite at 1590 and 1365 cm^{-1} are assigned to asymmetric C—O stretching and bending modes of H—C—O of the formate species respectively on the surface [36]. The intensity of the formate species bands change as a function of temperature with the protons for formate species being obtained from surface hydroxyl groups, whose intensity is high in the case of Ca perovskites. Bitter et al. proposed formation of similar kind of formate species at metal − support interface through bifunctional mechanism in DRM reaction over Pt/ZrO_2 catalyst [37]. They found that catalyst is not efficient if the carbonate species are not formed. The bands at 1075, 1440 and 1510 cm^{-1} were assigned to the formation of mono-dentate and poly-dentate carbonate formation over the perovskite surface respectively. In case of $BaZr_{0.8}Ni_{0.2}O_{3-\delta}$ perovskite, bands were observed at lower wave numbers: 1057, 1430 and 1475 cm^{-1} and are assigned to strongly bonded mono dentate and tridentate carbonates on the surface. The free $CO_3{}^{2-}$ ions have D_{3h} symmetry and hence expected to show single band around 1500 cm^{-1}, but bands are observed at lower than uncoordinated carbonates [16] and they loose trigonal symmetry of free carbonate ions. The main difference in IR spectra is in the intensity of O—H stretching frequencies at 3500–3750 cm^{-1} attributed to the terminal or polydentate hydroxyl species. The intensity of this band increases with temperature, which is present on the perovskite surface. In case of Ca perovskite the intensity of polydentate O—H band at 3630 cm^{-1} band is very sharp and highly intense compared to Ba perovskite. This shows that on Ca substituted perovskite, during the reaction, more hydroxyl species are produced and transported to metal – support interface to form formate intermediate species at a very high rate. Hence, Ca substituted perovskites shows stable conversion for longer hours. But, in case of Ba perovskite, CO_2 dissociative adsorption appears to be much lower and there is less formation of hydroxyl species for the DRM reaction to proceed. Eventually, accumulation of dehydrogenated carbon occurs on active Ni site which undergoes graphitization leading to the deactivation of the catalyst. Table S1 shows comparison of the IR results obtained for this study with those reported in literature. Based on all the aforementioned results, mechanism of dry reforming reaction over Ca and Ba perovskite surfaces is proposed in Scheme 1.

3.7. Characterization of spent catalysts

During dry reforming reaction, some of the side reactions are responsible for the carbon formation, which may lead to breakdown of the catalyst tablets, raising pressure drop across the catalysts bed. This can lead to the generation of hot spots, which are responsible for the uneven flow distribution [38]. Two major reactions that are responsible for the carbon formation are;

CH_4 decomposition ($CH_4 \rightarrow C + 2H_2$) (4)

Boudouard reaction ($2CO \rightarrow C + CO_2$) (5)

Characterization of spent catalyst will help to understand the carbon formation mechanism and types of carbon formed in relation to the nature of support. Hence, the spent catalysts were extensively characterized by XRD, TGA, TEM, XPS and Raman spectroscopy.

3.7.1. X-ray diffraction and Thermo gravimetric analysis of spent catalysts

The XRD of $MZr_{0.8}Ni_{0.2}O_{3-\delta}$ (M = Ca, Sr and Ba) catalysts that were used for 12 h of reaction are given in Fig. 9A. The diffraction patterns show that the structures are retained under the reaction conditions. However, spectra of Sr and Ba substituted samples show an additional peak at $2\theta = 26.4^{\circ}$, which is assigned to the graphitic carbon (JCPDS-41-1487). On the otherhand, only a small peak of negligible intensity was seen for $CaZr_{0.8}Ni_{0.2}O_{3-\delta}$ catalyst. Besides this carbon peak, small peaks that belong to alkaline earth carbonates were also observed. The intensity of the graphitic peak of $BaZr_{0.8}Ni_{0.2}O_{3-\delta}$ is relatively high compared to $SrZr_{0.8}Ni_{0.2}O_{3-\delta}$ after 12 h of DRM reaction. In addition,

Scheme 1. Schematic representation of reaction mechanism in the DRM process.

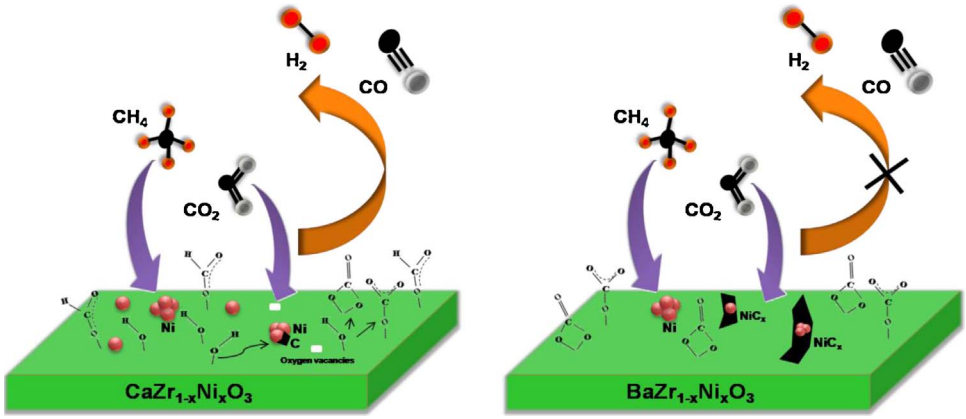

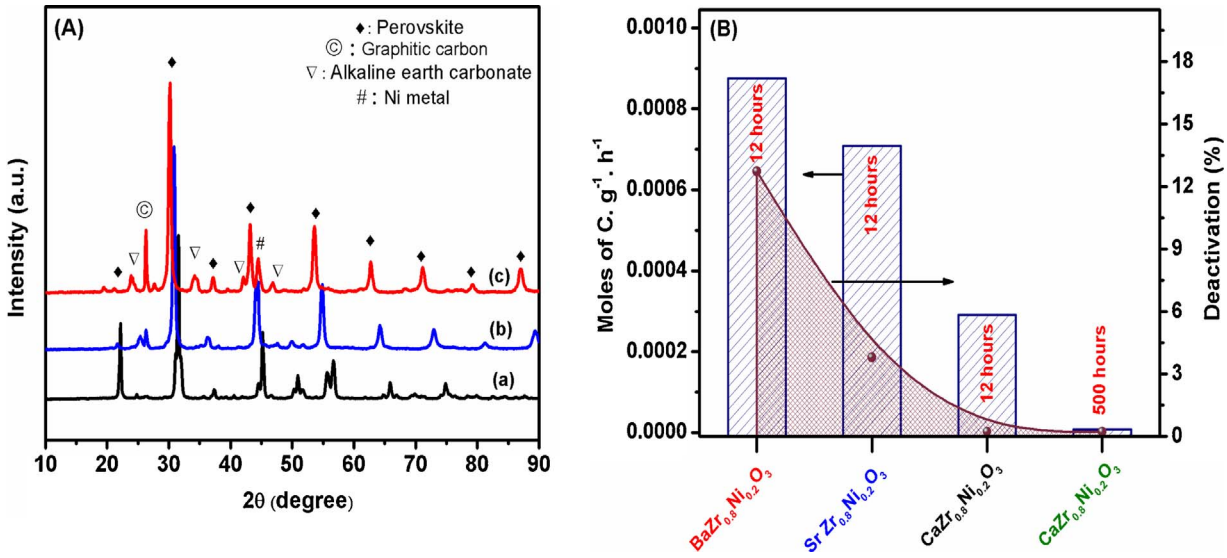

Fig. 9. Spent XRD of (A) $MZr_{0.8}Ni_{0.2}O_{3-\delta}$ (where M = (a) Ca, (b) Sr and (c) Ba) and (B) Coke estimated (moles of C g^{-1} h^{-1}) after DRM using TGA analysis.

presence of metallic Ni(111) was also observed, whose crystallite size was estimated using Scherrer's equation. The crystallite sizes of metallic Ni estimated for used $CaZr_{0.8}Ni_{0.2}O_{3-\delta}$ catalyst was13.4 nm, while it was 30 and 35.2 nm respectively for $SrZr_{0.8}Ni_{0.2}O_{3-\delta}$ and $BaZr_{0.8}Ni_{0.2}O_{3-\delta}$ catalysts.

Fig. S6 illustrates the XRD pattern of $CaZr_{0.8}Ni_{0.2}O_{3-\delta}$ catalyst prior to the reaction and after 12 h and 500 h of DRM reaction. No crystalline graphitic peak was observed even after 500 h of reaction, but a broad hump centered around 2θ = 26.4° was observed, which may be assigned to amorphous carbon. It appears that this amorphous carbon has hardly affected the activity of the catalyst, as CH_4 and CO_2 conversions remained same even after 500 h on stream. The metallic Ni crystallite size estimated after 500 h reaction was 15.2 nm, which was increased from 13.4 nm observed after 12 h of reaction. These results show that there is only small growth of Ni crystallite size, probably as a result of strong interaction between the metal and the support. These results clearly establish the reasons for high stability of $CaZr_{0.8}Ni_{0.2}O_{3-\delta}$ catalyst.

To further understand the extent of carbon formation after 12 h time on stream, all the three samples were subjected to TGA analysis. These

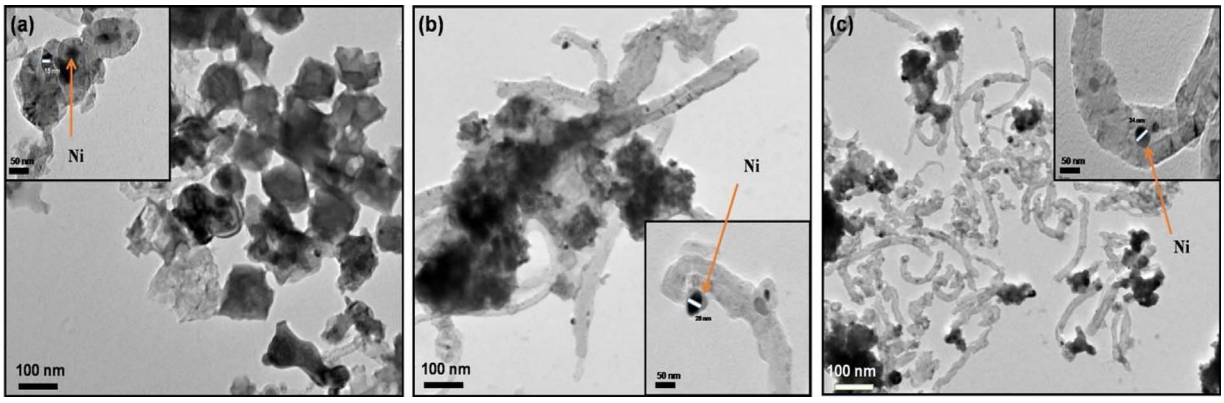

Fig. 10. TEM images of spent catalysts (a) $CaZr_{0.8}Ni_{0.2}O_{3-\delta}$, (b) $SrZr_{0.8}Ni_{0.2}O_{3-\delta}$, (c) $BaZr_{0.8}Ni_{0.2}O_{3-\delta}$.

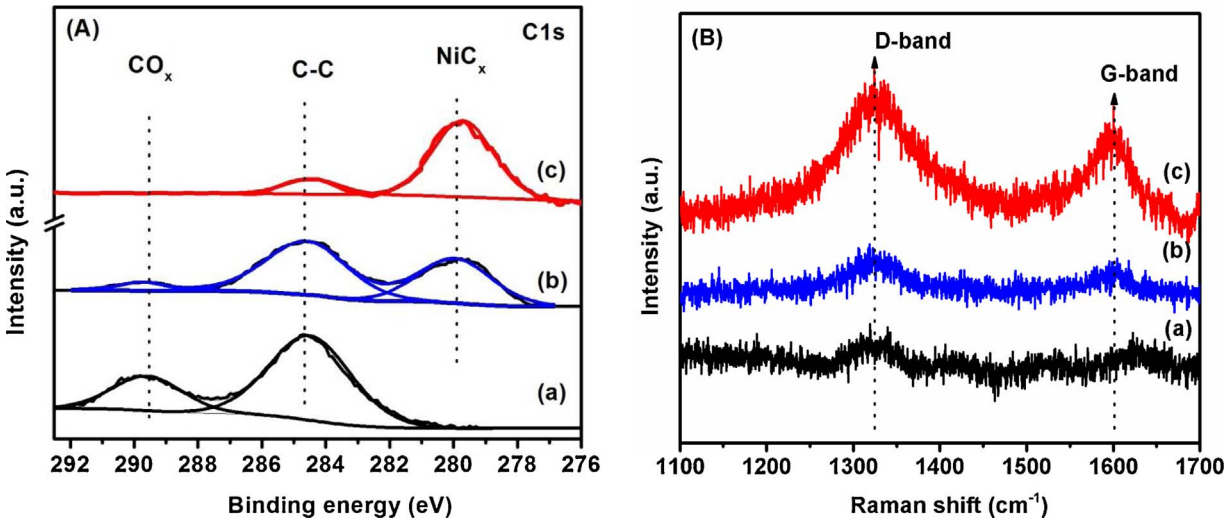

Fig. 11. (A) C1s XPS and (B) Raman spectra of spent $MZr_{0.8}Ni_{0.2}O_{3-\delta}$ perovskites after 12 h of TOS study, where M = (a) Ca, (b) Sr and (c) Ba.

experiments were carried out in presence of air and the carbon oxidized was calculated in terms of moles of carbon per gram of catalyst per hour. Results given in Fig. 9B illustrate that after 12 h of reaction, from $BaZr_{0.8}Ni_{0.2}O_{3-\delta}$ to $CaZr_{0.8}Ni_{0.2}O_{3-\delta}$ catalysts, the average carbon accumulation decreased per gram of catalyst. These results clearly show that alkaline earth cation present at the A site of catalyst plays significant role along with Ni particle size and oxygen defects for the coke accumulation during the DRM reaction. Zhang et al. reported that the rate of coke accumulation depends on the Ni particle size [39]. On the other hand, there was negligible coke formation in $CaZr_{0.8}Ni_{0.2}O_{3-\delta}$ catalysts even after 500 h of time on stream.

Ruckenstien and Wang et al. studied deactivation rate of Rh supported on various supports for dry reforming reaction. They found that catalysts are stable when balance is maintained between generation of carbon species and its oxidative removal under DRM conditions [40]. In case of $CaZr_{0.8}Ni_{0.2}O_{3-\delta}$ catalyst, probably this balance is maintained as carbon formation and its removal as CO/CO_2 are in equilibrium. Hence, it has not shown any observable deactivation even after 500 h of reaction.

3.7.2. HRTEM of spent catalysts

The type of carbon formed on the spent catalysts was analysed by TEM. The TEM micrographs expected to reveal presence of different types of carbon species formed on the three catalysts depending on the nature (basicity) of support, oxygen defects and Ni particle size (derived from CO chemisorption). Generally, three types of carbons can be seen, i.e., (i) amorphous carbon, (ii) graphitic carbon and (iii) multi walled carbon nanotubes (MWCNT). Carbon nanotubes can form through diffusion/elimination path way, which would result in the separation of active Ni species from the support [41]. On the otherhand, some pear shaped Ni particles placed at the tip of carbon nanotubes are expected to be still active for the reaction, while Ni particles that are incorporated into the carbon nanotubes may no longer participate in the reaction.

Fig. 10 shows TEM micrographs of samples tested for 12 h of reaction. The $SrZr_{0.8}Ni_{0.2}O_{3-\delta}$ and $BaZr_{0.8}Ni_{0.2}O_{3-\delta}$ catalysts show different kinds of surface carbon. These are amorphous carbon, filamentous carbon or carbon nanotubes with Ni at the tip and carbon nanotubes with embedded Ni particles inside. On the otherhand, on $CaZr_{0.8}Ni_{0.2}O_{3-\delta}$ catalyst, only amorphous carbon was seen, which is not expected to cause any deactivation of the catalyst during the DRM reaction. Over $SrZr_{0.8}Ni_{0.2}O_{3-\delta}$ catalyst, formation of CNT along with Ni particles in the range of 25–30 nm were seen, which were separated from the perovskite phase. Whereas, in case of $BaZr_{0.8}Ni_{0.2}O_{3-\delta}$ catalyst, formation of CNT with embedded Ni particles (30–40 nm) inside the tube were seen. These masked Ni particles can no longer be active for the DRM reaction. The TEM results further prove that the stability of $CaZr_{0.8}Ni_{0.2}O_{3-\delta}$ catalyst could be attributed to marginal growth of Ni crystallite size during the reaction, probably as a result of strong interaction between the metal and the support.

3.7.3. XPS analysis

The XRD and TEM analysis reveal the formation of different kinds of carbon species like amorphous carbon, carbon nanotubes and graphitic carbon during the DRM reaction over the catalysts. However, these techniques are inadequate to identify carbonate and carbide formation on the active metal surface, while XPS is highly useful for this purpose. Fig. 11A shows that the C1s spectra of all spent catalysts show a broad peak at 284.5 eV corresponding to the adsorbed carbon after exposure to ambient air or graphitic carbon. The intensity of this carbon peak (284.5 eV) is very high for $CaZr_{0.8}Ni_{0.2}O_{3-\delta}$ and $SrZr_{0.8}Ni_{0.2}O_{3-\delta}$ perovskite catalysts. Whereas, in case of $BaZr_{0.8}Ni_{0.2}O_{3-\delta}$ and $SrZr_{0.8}Ni_{0.2}O_{3-\delta}$ spent catalysts, additional binding energy (BE) peak at 280 eV was seen. This is at lower position than the normal nickel carbide peak (283.9 eV), associated with the NiC_x species on the surface [42]. These carbon species are formed on selective Ni faces of catalyst and are responsible for rapid deactivation of $BaZr_{0.8}Ni_{0.2}O_{3-\delta}$ and $SrZr_{0.8}Ni_{0.2}O_{3-\delta}$ catalysts. An additional higher binding energy peak seen at 289.5 eV indicates the formation of oxidized carbon species on $CaZr_{0.8}Ni_{0.2}O_{3-\delta}$ and $SrZr_{0.8}Ni_{0.2}O_{3-\delta}$ perovskite catalysts. [43].

The above results show that the formation of different types of carbon species depends on the nature of substituted alkaline earth cation in the perovskite lattice, metal dispersion and oxygen defects. This is further confirmed by analysing O 1s spectra of all the catalysts after reaction. Two main peaks labelled as O_L and O_s with various intensities can be seen in Fig. S7. The first peak at lower binding energy (530.4 eV) can be assigned to the O^{-2} ions which are part of perovskite lattice. The second peak at 532.5 eV corresponds to the surface oxygen containing species like carbonate and hydroxyl species [44]. The intensity of this peak is much higher for $CaZr_{0.8}Ni_{0.2}O_{3-\delta}$ catalyst compared to $SrZr_{0.8}Ni_{0.2}O_{3-\delta}$ or $BaZr_{0.8}Ni_{0.2}O_{3-\delta}$ perovskite catalysts. Table 3 provides information on binding energies of C1s and O1s and their assignments based on literature data [45]. The XPS binding energies obtained in this study are in agreement with the reported values in the literature

3.7.4. Raman analysis of spent catalysts

Raman spectroscopy is an effective tool to identify different types of

Table 3
C1s and O1s Binding energies of $MZr_{0.8}Ni_{0.2}O_{3-\delta}$ catalysts and their assignment.

Sample	C 1s B.E (eV)	Ref	Assignment	O 1s B.E (eV)	Ref	Assignment
$CaZr_{0.8}Ni_{0.2}O_{3-\delta}$	284.5 289.1	[43]	Hydrocarbon CO_x	530.2 532.5	[44]	Lattice oxygen Carbonate/hydroxyl groups
$SrZr_{0.8}Ni_{0.2}O_{3-\delta}$	280.0 284.6 289.2	[43,45]	Carbide Hydrocarbon CO_x	530.1 532.4	[44]	Lattice oxygen Carbonate/hydroxyl groups
$BaZr_{0.8}Ni_{0.2}O_{3-\delta}$	280.1 284.5	[42,45]	Carbide Hydrocarbon	530.3 532.3	[44,45]	Lattice oxygen Carbonate/hydroxyl groups

Table 4
Crystallite size of graphitic carbon calculated using Raman spectra.

Catalysts	I_D/I_G	I_G/I_D	Crystallite size of graphitic carbon (nm)[a]
$CaZr_{0.8}Ni_{0.2}O_{3-\delta}$ – 12 h	3.14	0.32	1.4
$SrZr_{0.8}Ni_{0.2}O_{3-\delta}$ – 12 h	2.10	0.47	2.1
$BaZr_{0.8}Ni_{0.2}O_{3-\delta}$ – 12 h	1.32	0.75	3.3
$CaZr_{0.8}Ni_{0.2}O_{3-\delta}$ – 500 h	1.86	0.53	2.4

[a] Estimated from I_G/I_D using formula crystallite size (nm) = $4.4[I_G/I_D]$.

carbon species present on the sample, i.e., carbon nanotubes, carbon films and synthetic diamond like carbon, after the DRM reaction [46]. There are many reports on various kinds of carbon species present on the catalyst surfaces [47]. Fig. 11B shows first order transition Raman spectra of spent Ca, Sr and Ba substituted $MZr_{0.8}Ni_{0.2}O_{3-\delta}$ perovskite catalysts. The peaks were seen at 1330 and 1600 cm^{-1} on all catalysts used for 12 h of DRM. These are assigned to D-band (1330 cm^{-1}) and G-band (1600 cm^{-1}). The band at 1330 cm^{-1}corresponds to the disorder induced band and it is allowed only if the selection rule breaks down (k = 0), which is coming from structural imperfections that exist in carbonaceous material [48]. This type of carbon is more reactive in reforming conditions. The G- band is attributed to stretching vibrations of sp^2 carbon in graphitic material and was designated E_{2g} mode. This band intensity depends on crystal size of the carbon. The shoulder peak at 1610 cm^{-1} (D′ band/E2g′ mode) is an indication of disordered graphitic material [49].

The intensity ratios of D- and G-bands (I_D/I_G) provide information about index of the crystalline order of graphitic carbon [50]. In Fig. S8, the intensities of D and G bands are compared for fresh $CaZr_{0.8}Ni_{0.2}O_{3-\delta}$ catalyst and catalysts used for reaction after 12 and 500 h of DRM reaction. It was observed that on increasing reaction time, only small increase in intensity of the disordered graphitic carbon was seen. The I_D/I_G values of all the spent catalyst samples were calculated. It was observed that I_D/I_G values decreased (Table 4) from $CaZr_{0.8}Ni_{0.2}O_{3-\delta}$ to $BaZr_{0.8}Ni_{0.2}O_{3-\delta}$ samples, with the Ba substituted sample showing very large graphitic carbon of 3.3 nm size just after 12 h of reaction. On the other hand, corresponding value for $CaZr_{0.8}Ni_{0.2}O_{3-\delta}$ catalyst was only 1.4 nm after 12 h of reaction, which has increased to 2.4 nm after 500 h DRM reaction.

After 12 h of reaction, I_D/I_G ratios were 3.1, 2.1 and 1.3 for used Ca, Sr and Ba substituted perovskite catalysts respectively. Whereas, I_D/I_G of Ca perovskite catalyst after 500 h reaction was 1.86, giving graphitic carbon crystallite size of 2.4 nm. These results clearly show that crystalline order of graphitic carbon depends on the nature of substituted alkaline earth cation and Ni particle size. The crystallite size of graphitic carbon calculated based on a reported method has been summarized in Table 4 [50]. Catalyst $CaZr_{0.8}Ni_{0.2}O_{3-\delta}$ shows very low crystallite size of graphitic carbon, which must be responsible for its high on-stream stability. Moreover, the smaller sized graphitic carbon can readily undergo oxidation or react with CO_2 ($C + CO_2 \rightarrow 2CO$) leading to long catalyst life.

4. Conclusions

Perovskite oxides $MZr_{1-x}Ni_xO_{3-\delta}$ (M = Ca, Sr and Ba; x = 0 and 0.2) were synthesized and evaluated as catalyst precursors in the dry reforming of methane. Changes in the lattice parameters, determined by XRD, confirmed that Ni is incorporated into $MZrO_3$ lattice. TPR of H_2 reveals that Ni in $CaZr_{0.8}Ni_{0.2}O_{3-\delta}$ perovskites was difficult to reduce as compared to corresponding Sr and Ba substituted samples. The results show that Ni reducibility, oxygen storage, Ni dispersion and surface area of catalyst play vital role in achieving good DRM activity and also helps in retaining the activity for long hours on stream. Among the catalysts, $CaZr_{0.8}Ni_{0.2}O_{3-\delta}$ seems to have all desirable characteristics, as it shows superior activity and sustains its activity even after 500 h. Transient pulse experiments suggest that redox property of the support is vital for the removal of carbon species formed during CH_4 decomposition and also in recovering the lattice oxygen through CO_2 activation. Infrared results revealed that adsorbed intermediates like formate and surface hydroxyl species are crucial for minimisation of carbon in dry reforming reaction. Characterization of spent catalysts, used for dry reforming reaction, show high growth of graphitic carbon on $SrZr_{0.8}Ni_{0.2}O_{3-\delta}$ and $BaZr_{0.8}Ni_{0.2}O_{3-\delta}$ catalysts, thus leading to their rapid deactivation. XPS analysis confirms the formation of NiC_x species on these catalysts, which must be also responsible for their rapid deactivation. This study clearly establishes that $CaZr_{0.8}Ni_{0.2}O_{3-\delta}$ is a highly active and durable catalyst for dry reforming of methane with immense potential for commercial exploitation.

Acknowledgments

Srikanth Dama, Richa Bobade and Hanmant R. Gurav acknowledge Council of Scientific and Industrial Research, New Delhi, for providing senior research fellowship. Authors also acknowledge financial support by CSIR, New Delhi through network project CSC-0102

Appendix A. Supplementary data

Supplementary data associated with this article can be found, in the online version, at http://dx.doi.org/10.1016/j.apcatb.2017.10.048.

References

[1] T.H. Oh, Carbon capture and storage potential in coal-fired plant in Malaysia – a review, Renew. Sust. Energy Rev. 14 (2010) 2697–2709.
[2] Z.L. Zhang, X.E. Verykios, Mechanistic aspects of carbon dioxide reforming of methane to synthesis gas over Ni catalysts, Catal. Lett. 38 (1996) 175–179.
[3] L. Kapokova, S. Pavlova, R. Bunina, G. Alikina, T. Krieger, A. Ishchenko, V. Rogov, V. Sadykov, Dry reforming of methane over $LnFe_{0.7}Ni_{0.3}O_{3-\delta}$ perovskites: Influence of Ln nature, Catal. Today 164 (2011) 227–233.
[4] H.R. Gurav, S. Dama, V. Samuel, S. Chilukuri, Influence of preparation method on activity and stability of Ni catalysts supported on Gd doped ceria in dry reforming of methane, J. CO_2 Util. 20 (2017) 357–367.
[5] H.Y. Wang, E. Ruckenstein, Carbon dioxide reforming of methane to synthesis gas over supported rhodium catalysts: the effect of support, Appl. Catal. A: Gen. 204 (2000) 143–152.
[6] N. Sun, X. Wen, F. Wang, W. Peng, N. Zhao, F. Xiao, W. Wei, Y. Sun, J. Kang, Catalytic performance and characterization of Ni-CaO-ZrO_2 catalysts for dry reforming of methane, Appl. Surf. Sci. 257 (2011) 9169–9176.

[7] J.G. Zhang, H. Wang, A.K. Dalai, Development of stable bimetallic catalysts for carbon dioxide reforming of methane, J. Catal. 249 (2007) 300–310.
[8] G.S. Gallego, F. Mondragón, J. Barrault, J.M. Tatibouet, C. Batiot-Dupeyrat, CO_2 reforming of CH_4 over La-Ni based perovskite precursors, Appl. Catal. A: Gen. 311 (2006) 164–171.
[9] S. Corthals, J. Van Nederkassel, J. Geboers, H. De Winne, J. Van Noyen, B. Moens, B. Sels, P. Jacobs, Influence of composition of $MgAl_2O_4$ supported $NiCeO_2ZrO_2$ catalysts on coke formation and catalyst stability for dry reforming of methane, Catal. Today 138 (2008) 28–32.
[10] M. Rezaei, S.M. Alavi, S. Sahebdelfar, P. Bai, X. Liu, Z.-F. Yan, The effect of CeO_2 on the surface and catalytic properties of Pt/CeO_2-ZrO_2 catalysts for methane dry reforming, Appl. Catal. B: Environ. 77 (2008) 346–354.
[11] Y.-G. Chen, K. Tomishige, K. Yokoyama, K. Fujimoto, Promoting effect of Pt, Pd and Rh noble metals to the $Ni_{0.03}Mg_{0.97}O$ solid solution catalysts for the reforming of CH_4 with CO_2, Appl. Catal. A: Gen. 165 (1997) 335–347.
[12] V. Garcia, J.J. Fernandez, W. Ruiz, F. Mondragon, A. Moreno, Effect of MgO addition on the basicity of Ni/ZrO_2 and on its catalytic activity in carbon dioxide reforming of methane, Catal. Commun. 11 (2009) 240–246.
[13] E. Pietri, A. Barrios, O. Gonzalez, M.R. Goldwasser, M.J. Perez Zurita, M.L. Cubeiro, J. Goldwasser, L. Leclercq, G. Leclercq, L. Gingembre, Perovskites as catalysts precursors for methane reforming: Ru based catalysts, Stud. Surf. Sci. Catal. 136 (2001) 381–386.
[14] X. Li, J.S. Chang, M. Tian, S.E. Park, CO_2 reforming of methane over modified Ni/ZrO_2 catalysts, Appl. Organomet. Chem. 15 (2001) 109–112.
[15] P. Kumar, Y. Sun, R.O. Idem, Nickel-based ceria, zirconia, and ceria-zirconia catalytic systems for low-temperature carbon dioxide reforming of methane, Energy Fuel 21 (2007) 3113–3123.
[16] P. Ferreira-Aparicio, I. Rodríguez-Ramos, J.A. Anderson, A. Guerrero-Ruiz, Mechanistic aspects of the dry reforming of methane over ruthenium catalysts, Appl. Catal. A: Gen. 202 (2000) 183–196.
[17] A.E. Pasto, R.E. Condrate, Advances in Raman Spectroscopy 1 Heyden & Son, London, 1973, p. 196.
[18] K. Boobalan, A. Varun, R. Vijayaraghavan, K. Chidambaram, U. Kamachi Mudali, Facile, scalable synthesis of nanocrystalline calcium zirconate by the solution combustion method, Ceram. Int. 40 (2014) 5781–5786.
[19] M. Tarrida, H. Larguem, M. Madon, Structural investigations of (Ca, Sr)ZrO_3 and Ca(Sn Zr)O_3 perovskite compounds, Phys. Chem. Miner. 36 (2009) 403–413.
[20] V.M. Orera, C. Pecharroman, J.I. Pena, R.I. Merino, C.J. Serna, Vibrational spectroscopy of $CaZrO_3$ single crystals, J. Phys. Condens. Matter 10 (1998) 7501–7510.
[21] C.H. Perry, D.J. MacCarthy, G. Rupprecht, Dielectric dispersion of some perovskite zirconates, Phys. Rev. 138A (5) (1965) 1537–1538.
[22] Ph. Colomban, C. Tran, O. Zaafrani, A. Slodczyk, Aqua oxyhydroxycarbonate second phases at the surface of Ba/Sr-based proton conducting perovskites: a source of confusion in the understanding of proton conduction, J. Raman Spectrosc. 44 (2013) 312–320.
[23] A. Slodczyk, Ph. Colomban, S. Willemin, O. Lacroix, B. Sala, Indirect Raman identification of the proton insertion in the high-temperature [Ba/Sr][Zr/Ti]O_3-modified perovskite protonic conductors, J. Raman Spectrosc. 40 (2009) 513–521.
[24] C.S. Bai, S. Soled, R. Kershaw, K. Dwight, A. Wold, The preparation and characterization of the phases formed by the reactions of nickel and lanthanum nitrates with magnesium aluminate, J. Solid State Chem. 100 (1992) 307–312.
[25] S.M.A. Rodulfo-Baechler, W. Pernia, I. Aray, H. Figueroa, S.L. Gonzalez-Cortes, Influence of lanthanum carbonate phases of Ni/$La_{0.98}Sr_{0.02}O_x$ catalyst over the oxidative transformation of methane, Catal. Lett. 112 (2006) 231–237.
[26] F. Rohr, S.D. Peter, E. Lox, M. Kogel, A. Sassi, L. Juste, C. Rigaudeau, G. Belot, P. Gelin, M. Primet, On the mechanism of sulphur poisoning and regeneration of a commercial gasoline NO_x-storage catalyst, Appl. Catal. B 56 (2005) 201–212.
[27] J. Rynkowski, P. Samulkiewicz, A.K. Ladavos, P.J. Pomonis, Catalytic performance of reduced $La_{2-x}Sr_xNiO_4$ perovskite-like oxides for CO_2 reforming of CH_4, Appl. Catal. A 263 (2004) 1–9.
[28] A. Yan, M. Yang, Z. Hou, Y. Dong, M. Cheng, Investigation of $Ba_{1-x}Sr_xCo_{0.8}Fe_{0.2}O_{3-(}$ as cathodes for low-temperature solid oxide fuel cells both in the absence and presence of CO_2, J. Power Sources 185 (2008) 76–84.
[29] C.M. Chan, R. Aris, W.H. Weinberg, An analysis of thermal desorption mass spectra, Appl. Surf. Sci. 1 (1978) 360–376.
[30] K. Li, M. Haneda, M. Ozawa, Oxygen release-absorption properties and structural stability of $Ce_{0.8}Fe_{0.2}O_{2-x}$, J. Mater. Sci. 48 (2013) 5733–5743.
[31] S. Pei, M.S. Kleefisch, T.P. Kobylinski, J. Faber, C.A. Udovich, V. Zhang-McCoy, B. Dabrowski, U. Balachandran, R.L. Mieville, R.B. Poeppel, Failure mechanisms of ceramic membrane reactors in partial oxidation of methane to synthesis gas, Catal. Lett. 30 (1995) 201–212.
[32] G.S. Gallego, C.B. Dupeyrat, J. Barrault, E. Florez, F. Mondragon, Dry reforming of methane over $LaNi_{1-y}B_yO_{3\pm(}$ (B = Mg, Co) perovskites used as catalyst precursor, Appl. Catal. A: Gen. 334 (2008) 251–258.
[33] J.D.A. Bellido, E.M. Assaf, Effect of the Y_2O_3-ZrO_2 support composition on nickel catalyst evaluated in dry reforming of methane, Appl. Catal. A: Gen. 352 (2009) 179–187.
[34] P. Ferreira-Aparicio, C. Marquez-Alvarez, I. Rodríguez-Ramos, Y. Schuurman, A. Guerrero-Ruiz, C. Mirodatos, A transient kinetic study of the carbon dioxide reforming of methane over supported Ru catalysts, J. Catal. 184 (1999) 202–212.
[35] X. Yi-de, Y. Lin, G. Xie-Xian, An Insitu FTIR study on the interaction and reaction of CH_4 and O_2 with the surface of SrO-La_2O_3/CaO catalysts, J. Nat. Gas Chem. 8 (1999) 18–34.
[36] M.M. Schubert, H.A. Gasteiger, R.J. Behm, Surface formates as side products in the selective CO oxidation on Pt/(-Al_2O_3, J. Catal. 172 (1997) 256–258.
[37] J.H. Bitter, K. Seshan, J.A. Lercher, Mono and bifunctional pathways of CO_2/CH_4 reforming over Pt and Rh based catalysts, J. Catal. 176 (1998) 93–101.
[38] A.M. Gadalla, B. Bower, The role of catalyst support on the activity of nickel for reforming methane with CO_2, Chem. Eng. Sci. 43 (1988) 3049–3062.
[39] Z.L. Zhang, X.E. Verykios, Carbon dioxide reforming of methane to synthesis gas over supported Ni catalysts, Catal. Today 21 (1994) 589–595.
[40] E. Ruckenstein, H.Y. Wang, Carbon deposition and catalytic deactivation during CO_2 reforming of CH_4 over Co/γ-Al_2O_3 catalysts, J. Catal. 205 (2002) 289–293.
[41] C. Wang, N. Sun, N. Zhao, F. Xiao, W. Wei, J. Zhang, T. Zhao, Y. Sun, C. Sun, H. Liu, C.E. Snape, The properties of individual carbon residuals and their influence on the deactivation of Ni-CaO-ZrO_2 catalysts in CH_4 dry reforming, Chem. Cat. Chem. 6 (2014) 640–648.
[42] J.W. Shabaker, D.A. Simonetti, R.D. Cortright, J.A. Dumesic, Sn-modified Ni catalysts for aqueous-phase reforming: characterization and deactivation studies, J. Catal. 231 (2005) 67–76.
[43] M. Ni, B.D. Ratner, Differentiating calcium carbonate polymorphs by surface analysis techniques −an XPS and TOF-SIMS study, Surf. Interface Anal. 40 (2008) 1356–1361.
[44] J. Requies, M.A. Cabrero, V.L. Barrio, M.B. Güemez, J.F. Cambra, P.L. Arias, F.J. Pérez-Alonso, M. Ojeda, M.A. Peña, J.L.G. Fierro, Partial oxidation of methane to syngas over Ni/MgO and Ni/La_2O_3 catalysts, Appl. Catal. A: Gen. 289 (2005) 214–223.
[45] T. Ujvari, A. Toth, G.J. Kovacs, G. Safran, O. Geszti, G. Radnoczi, I. Bertoti, Composition, structure and mechanical property analysis of DC sputtered C-Ni and CN_x-Ni nano-composite layers, Surf. Interface Anal. 36 (2004) 760–764.
[46] C. Klinke, R. Kurt, J.M. Bonard, Raman spectroscopy and field emission measurements on catalytically grown carbon nanotubes, J. Phys. Chem. B 106 (2002) 11191–11195.
[47] F. Tuinstra, J.L.J. Koeing, Raman spectrum of graphite, Chem. Phys. 53 (1970) 1126–1130.
[48] A. Cuesta, P. Dhamelincourt, J. Laureyns, A.M. Alonso, J.M.D. Tascon, Raman microprobe studies on carbon materials, Carbon 32 (1994) 1523–1532.
[49] R. Tsu, J.H. Gonzalez, I.C. Hernandez, Observation of splitting of the E2 g mode and two phonon spectrum in graphites, Solid State Commun. 27 (1978) 507–510.
[50] T. Jawhari, A. Roid, J. Casado, Raman spectroscopic characterisation of some commercially available carbon black materials, Carbon 33 (1995) 1561–1565.